Exploring the Validity and Limitations of the Mott-Gurney Law for Charge-Carrier Mobility Determination of Semiconducting Thin-Films

Jason A. Röhr[1,2,*], Davide Moia[1], Saif A. Haque[2], Thomas Kirchartz[3,4,*] and Jenny Nelson[1]

[1]*Department of Physics & Centre for Plastic Electronics, Imperial College London, South Kensington Campus, London SW7 2AZ, United Kingdom*
[2]*Department of Chemistry & Centre for Plastic Electronics, Imperial College London, South Kensington Campus, London SW7 2AZ, United Kingdom*
[3]*IEK5-Photovoltaics, Forschungszentrum Jülich, 52425 Jülich, Germany*
[4]*Faculty of Engineering and CENIDE, University of Duisburg-Essen, Carl-Benz-Strasse 199, 47057 Duisburg, Germany*

Using drift-diffusion simulations, we investigate the voltage dependence of the dark current in single carrier devices typically used to determine charge-carrier mobilities. For both low and high voltages, the current increases linearly with the applied voltage. Whereas the linear current at low voltages is mainly due to space charge in the middle of the device, the linear current at high voltage is caused by charge-carrier saturation due to a high degree of injection. As a consequence, the current density at these voltages does not follow the classical square law derived by Mott and Gurney, and we show that for trap-free devices, only for intermediate voltages, a space-charge-limited drift current can be observed with a slope that approaches two. We show that, depending on the thickness of the semiconductor layer and the size of the injection barriers, the two linear current-voltage regimes can dominate the whole voltage range, and the intermediate Mott-Gurney regime can shrink or disappear. In this case, which will especially occur for thicknesses and injection barriers typical for single-carrier devices used to probe organic semiconductors, a meaningful analysis using the Mott-Gurney law will become unachievable, because a square-law fit can no longer be achieved, resulting in the mobility being substantially underestimated. General criteria for when to expect deviations from the Mott-Gurney law when used for analysis of intrinsic semiconductors are discussed.

1. Introduction

The space-charge-limited current (SCLC) measurement of charge carrier mobilities relies on the interpretation of current voltage characteristics of single-carrier devices. The measurement is simple to perform, which makes SCLC a convenient method for investigating charge transport properties of semiconductors[1][2][3][4]. In addition, single-carrier devices used for SCLC measurements are of similar architecture to solar cells and diodes, allowing for the determination of the charge-carrier mobility of a device with similar film thickness, similar processing history, and therefore similar morphology. This allows for a direct comparison of the films used to measure charge transport and the films used for the optoelectronic components. This is in contrast to other popular charge transport characterisation techniques, such as time-of-flight mobility measurements which require very thick devices, and field-effect-transistor mobility measurements which require a lateral device structure and hence probe the lateral charge transport.

The obtained SCLC data is however prone to misinterpretation, and identifying the correct model for interpreting the measured current density-voltage (J-V) curves is a critical matter[5]. The widely used Mott-Gurney (MG) law[6] has been proposed as a good model for interpreting SCLC of devices that satisfy the following conditions: i) The semiconductor layer being probed is undoped and trap free, and ii) is sandwiched between two Ohmic contacts (even though Ohmic contacts are not always well defined). Furthermore, iii) diffusion contributions to the current must be negligible, which may be the case only for certain voltage ranges, even for devices that satisfy i) and ii). In this work we use the term 'ideal' for devices satisfying conditions i) and ii). However, the J-V curves from real single-carrier devices are usually affected by the non-ideal features of the material such as charge-carrier traps, energetic disorder or doping, and also by the non-ideality of the single-carrier device, such as the effect of injection barriers and built-in voltages arising from the choice of contacts[7][8]. These non-ideal features lead to deviations

between the actual mobility and the one determined from the MG law as well as to deviations between the actual shape of the J-V curve and the one predicted by the MG law.

In previous studies, attempts have been made to find alternative models to fit SCLC data to account for non-ideal behaviour. For example, analytical equations have been expanded from the MG law to give qualitative explanations to the observed effects of traps, such as Rose's and Lampert's approach of defining an effective mobility when a discrete level of traps is present[9][10], and the Mark-Helfrich equation which describes current in the Mott-Gurney regime when a shallow exponential distribution of traps is present[7]. Equations have also been derived to explain Poole-Frenkel like effects, such as the Murgatroyd equation[11]. However, since all of these equations ignore the diffusion part of the current, which is the part of the current which is most heavily influenced by the presence of traps and disorder, they must be approached with caution when used for SCLC analysis[12][13]. A number of other studies have utilized a more sophisticated model to analyse SCLC through the use of drift-diffusion simulations[14][15][16][17][18][19], although the majority of SCLC measurements is still, to this date, being analysed using analytical models.

As mentioned above, a vast amount of effort has been put into adapting the simple MG theory to account for non-ideal features such as traps. However, none of the previous studies have directly addressed the fundamental question of whether the MG law is in fact suitable for analysis of ideal materials, i.e., whether the MG law can accurately describe the response of ideal materials, without traps or energetic disorder, for which it was originally derived. The model on which the MG law is based implies that the electric field at the injecting contact is zero. This causes the charge-carrier density in the semiconductor, at this point, to tend to infinity and decrease towards the extracting contact, following an $\sqrt{x^{-1}}$ dependence, where x is the spatial positon from the injecting contact (regardless of the magnitude of the applied voltage). This is a non-physical situation resulting from the boundary conditions used, and does not reflect what is happening in a real device. By not considering the metal-semiconductor contacts properly, the MG law does not correctly account for charge-carrier injection from the metal, beyond the equilibrium charge carrier density, neither without an applied bias nor when a very large bias is applied. For this reason, the MG theory is not able to account for the current at low voltages[20][21], and for the accumulation of charge-carriers beyond the MG description, and eventual charge-carrier saturation (large uniform density across the length of the semiconducting layer) inside the single-carrier device when a large voltage is applied[22]. Accounting for the phenomena responsible for the current-voltage response at both at low and high voltages, is important for a complete description of the charge-transport through a single-carrier device.

In the present study we address the applicability of the MG law to the case of an ideal material. Our analysis rests particularly on the physical validity of the boundary conditions assumed in the MG law derivation and on the importance of charge saturation in devices of typical thicknesses and with typical injection barrier heights of those that are studied experimentally in the community. Through drift-diffusion simulations the current density-voltage and charge-carrier density profiles of ideal and non-ideal single-carrier devices of intrinsic semiconductors are investigated. We show that the charge-carrier accumulation must be accounted for when the semiconductor film is thin, appreciable voltages are applied and/or when injection barriers are present, since the linear voltage regimes will dominate the J-V curves and a fit with the MG law can no longer be achieved. The accuracy of the MG law is then evaluated for the simulated single-carrier devices when saturation currents dominate, and it is shown that when the MG law is nevertheless used, even though a direct fit cannot be achieved, the obtained charge-carrier mobility will be underestimated by up to several orders of magnitude. The findings of the study are particularly important when analysing SCLC measurements of organic semiconductors, when the thickness of the semiconducting layer is thin (<100 nm)[19][23] and the injection barriers between the metal contacts and the semiconductor are relatively large (>0.1 eV)[24]. The findings in this study are, however, not limited to organic semiconductors, but are relevant for all intrinsic semiconductors probed by SCLC using single-carrier devices.

2. Single-carrier devices

Single-carrier devices, used to measure SCLC, consist of a semiconductor sandwiched between two electrodes. The energetics of the interface between the semiconductor and the electrodes are briefly reviewed here. When an interface is formed between a metal and an intrinsic semiconductor, given that the value of the work function of the metal, or the metal Fermi energy, $E_{\mathrm{F}}^{\mathrm{metal}}$, is approximately equal to either the conduction band energy, E_{C}, or valence band edge energy, E_{V}, either electrons or holes are injected into the semiconductor from the metal forming either a negative or positive space-charge layer at the interface (shown for electrons in fig. 1a). This happens in order to equilibrate the Fermi level across the interface (we refer to the charge carriers injected in this way as the equilibrium charge carriers). The depth of the space-charge layer due to this charge-carrier injection is governed by the Debye screening length (see fig. 1a). The authors define the interface between a metal and a semiconductor as shown in fig 1a as an Ohmic contact.

In the case of an electron injecting interface, if the metal work function is slightly larger than the electron affinity ($E_{\mathrm{vac}} - E_{\mathrm{C}}$), i.e., the metal Fermi energy $E_{\mathrm{F}}^{\mathrm{metal}}$ is a few meV deeper than E_{C} of the semiconductor, an injection barrier, $q\phi_{\mathrm{inj}}$, is formed. Such an interface is shown in fig. 1b, and the authors define such a contact as a non-Ohmic contact.

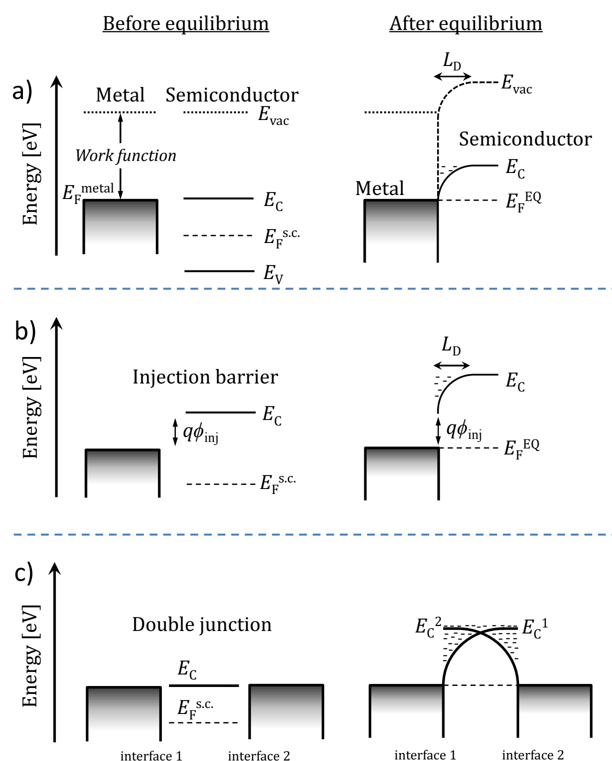

Figure 1 – a) Metal/(intrinsic)semiconductor interface prior to and after equilibrium with perfect match between conduction band edge ($\boldsymbol{E}_{\mathbf{C}}$) and metal Fermi energy ($\boldsymbol{E}_{\mathbf{F}}^{\mathbf{metal}}$). b) Difference between $\boldsymbol{E}_{\mathbf{F}}^{\mathbf{metal}}$ and $\boldsymbol{E}_{\mathbf{C}}$ will lead to an injection barrier ($\boldsymbol{\phi}_{\mathbf{inj}}$). c) Metal/semiconductor/metal interface prior to and after equilibrium (E_{C}^{1} and E_{C}^{2} represent the conduction band edges arising from interface 1 and 2, respectively). The depth of the space-charge region, as determined from the Debye length ($\boldsymbol{L}_{\mathbf{D}}$), is shown in a and b).

In the case of a metal/semiconductor/metal device, where the semiconductor layer is thinner than twice the space-charge layer thickness (a situation which is also called overlapping contacts[25][26]), charge carriers are injected from both electrodes in great excess of the intrinsic carrier density across the length of the device[27]. Such a device, as shown in fig. 1c, is completely governed by the equilibrium electrons, and the device is called an electron-only device. Since injection of further charge carriers, when applying a bias voltage across the device, is of the same type as the equilibrium charge carriers in the device, the current flowing through the device is space-charge-limited and does not depend on intrinsic charge carriers.

A schematic of a finished symmetric single-carrier device with Ohmic contacts is shown in fig. 2a. It is here important to mention that an additional barrier for electron flow exists, namely the internal diffusion barrier, $q\phi_{\mathrm{diff}}$, which is defined as the difference between the conduction band edge energy and Fermi level at the virtual electrode, which is the point of vanishing electric field (see fig. 2a). Even though charge-carriers have entered the device through the injection barrier, which for an Ohmic contact could be zero, the charge-carriers must cross the diffusion barrier for current to flow through the device. This results in a total barrier height hindering charge-transport which can be treated as a sum of the internal diffusion barrier height and the injection barrier height, $q\phi_{\mathrm{tot}} = q\phi_{\mathrm{diff}} + q\phi_{\mathrm{inj}}$[28]. As will be seen below, as the voltage is applied across the device, $q\phi_{\mathrm{diff}}$ will reduce in height while $q\phi_{\mathrm{inj}}$ will remain constant.

3. Analytical theory

The following sections review the analytical expressions that describe current flow through intrinsic semiconductors placed in ideal and non-ideal single-carrier devices; in the low voltage regime (the moving electrode equation), the intermediate voltage regime (the MG law), and in the high voltages regime (the saturation current equation).

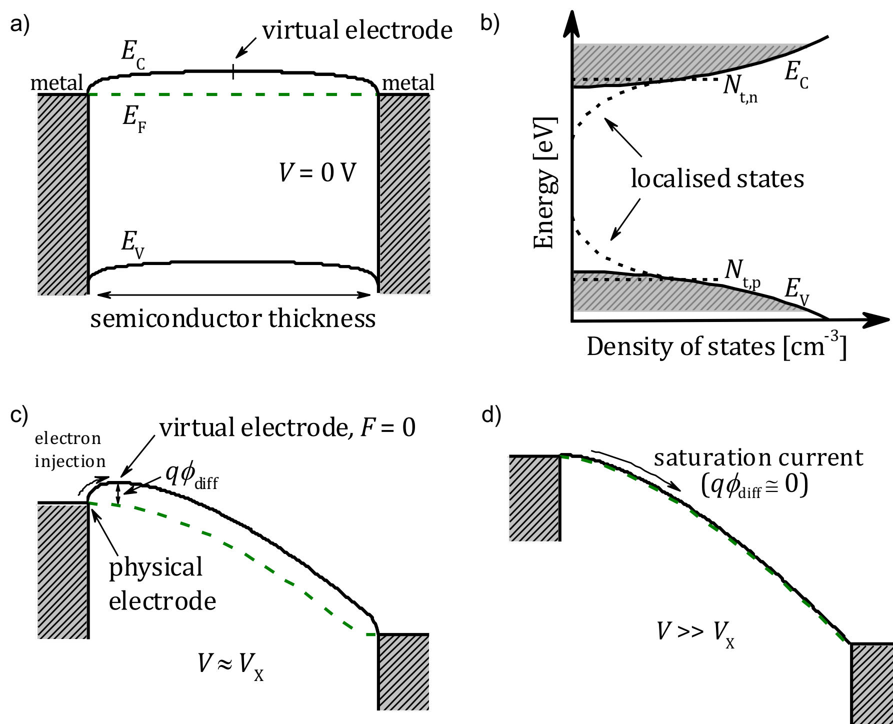

Figure 2 – a) Schematic of energy level diagrams of an electron-only at equilibrium showing the position of the virtual electrode with black solid lines being the spatial conduction and valence band edge energies, and the green

dashed line being the semiconductor Fermi level. b) Density of states profiles of the studied semiconductors with traps ($\boldsymbol{N_t}$ is the trap density at the connection points between the parabolic density of states and the tails). c) Energy level diagrams under a moderately applied voltage, $V \cong V_X$, where V_x is the voltage onset to drift dominated currents. The virtual electrode is shown to move towards the physical electrode. d) At a large applied voltage ($V >> V_X$) the carrier density is saturated across the device.

3.1. The moving electrode equation

When a low voltage is applied across an intrinsic and symmetric single-carrier device (fig. 2a), a linear *J*-*V* behaviour is observed[20][21][29]. This current is not due to the intrinsic charge-carrier density, but rather due to the equilibrium charge-carrier density in the middle of the device[30], and is therefore not a true Ohmic current[27]. This linear *J*-*V* behaviour is observed until the condition where the virtual electrode, moves to the physical electrode at the device boundary (fig. 2a and c). Since the condition for when this linear current is observed happens when the virtual electrode moves, we denote the current as the moving electrode (ME) current. The relatively unknown equation governing the ME current was first presented by R. de Levie *et al*[20] and later by Grinberg and Luryi[21]. In the case of an electron-only device, where only electron transport is probed, the ME equation is given by

$$J = 4\pi^2 \frac{k_B T}{q} \mu_n \varepsilon_0 \varepsilon_r \frac{V}{L^3}, \quad (1)$$

where $k_B T$ is the thermal energy, q is the elementary charge, μ_n is the electron mobility (assumed independent of the charge-carrier density and electric field), $\varepsilon_0 \varepsilon_r$ is the permittivity, V is the applied voltage (up to around 0.1 V) and L is the semiconductor thickness. Given that the temperature, the relative permittivity and the thickness of the sample is known, the ME equation (eq. 1) can, in principle, be fitted to the low voltage regime and the mobility can be extracted. It is important to note that the ME equation only correctly gives the current density at low voltages when the semiconductor is trap free and doping free and when the current is not limited by poor injection from the metal contacts.

The spatial dependence of the charge-carrier density neither increases nor shifts significantly whilst the current follows the ME equation. The energy landscape of the single-carrier device is, for that reason, well represented by fig. 2a whilst the ME current is flowing.

3.2. The Mott-Gurney law

When a large enough voltage is applied across a single-carrier device, so that the virtual electrode coincides with the physical electrode, $q\phi_{\text{diff}}$ is approximately zero, and the current across the device will mainly be governed by drift. The current can in this case be described by the MG law which, for the case of an electron-only device, is given by[6],

$$J = \frac{9}{8} \mu_n \varepsilon_0 \varepsilon_r \frac{V^2}{L^3}, \quad (2)$$

The charge-carrier mobility of the electrons can in principle be obtained by fitting with the MG law (eq. 2) to the *J*-*V* curve obtained from the SCLC measurement in the region where $J \propto V^2$, i.e., in the MG voltage regime. The MG law is only applicable given that a number of assumptions are true: i) the intrinsic carrier concentration is negligible when current is flowing, meaning that the current will mainly be governed by the equilibrium charge-carrier density and the injected charge carriers due to an applied voltage; ii) both the contacts for injection and extraction are Ohmic, meaning that $q\phi_{\text{inj/ext}} \cong 0$ eV or injection barriers are not affecting the current, and charge carriers are always available to enter and leave the device, i.e., the metals act as electron

reservoirs; iii) the material is defect free and free from energetic disorder, and finally; iv) the current density is governed by drift only, which implies the previously mentioned condition of vanishing electric field at the device interface.

Assumption i) is justified in the discussion of fig. 1. The other assumptions are however generally not true: Regarding assumption ii), we define our contact potentials as the difference between $E_{\mathrm{F}}^{\mathrm{metal}}$ and the respective band-edge energy (here the conduction band for an electron-only device, as shown in fig 1c,

$$q\phi_{\mathrm{inj}} = E_{\mathrm{C}}(x=0) - E_{\mathrm{F}}^{\mathrm{metal}}(x=0). \quad (3)$$

Realising Ohmic contacts to a semiconductor is not easily achieved, as surface states can pin the Fermi level in the sub-gap region. Furthermore, low work function materials, which are commonly used as electron selective contacts to organic materials, such as Ca (2.9 eV), Ba (2.7 eV) and Al (4.1 eV), are highly reactive with the ambient atmosphere, causing them to oxidize, usually resulting in a change in work function. Assumption iii) is usually not true since many semiconducting materials are semi-crystalline or amorphous which means they are usually not defect free. Such defects can act as trap sites or give rise to unintentional doping, which will either decrease (traps) or increase (doping) the overall magnitude if the current whilst drastically changing the shape of the J-V curve[31][32]. As a consequence of iv) the electric field will increase within the electron-only device as,

$$F(x) = -\sqrt{\frac{2Jx}{\mu_n \varepsilon_0 \varepsilon_{\mathrm{r}}}}, \quad (4)$$

where x is the position from the injecting contact. The charge carrier density for electrons can then be obtained through Gauss' law as,

$$n(x) = \frac{1}{q}\sqrt{\frac{J\varepsilon_0 \varepsilon_{\mathrm{r}}}{2\mu_n x}}. \quad (5)$$

It is important to note that the analytical expression of the charge-carrier density in the MG regime (eq. 5) tends to infinity at the injecting contact. Like previously mentioned, this is a non-physical situation resulting from the boundary conditions imposed on the electric field at the device boundary ($F = 0$ at $x = 0$). Having a finite charge-carrier density at the device boundaries rather than allowing the charge-carrier density to extend to infinity will have an influence on the current density.

3.3. The saturation current equation

At high voltages, a large density of charge carriers is injected into a single-carrier device to an extent where the charge-carrier density across the device is uniform (fig. 2d). This is called the charge-carrier saturation limit, and is also referred to as the injection limit. This is distinct from the limit, sometimes described in the literature, where the velocity saturates along with constant field and uniform carrier density in the situation we describe, velocity and field are not uniform. Henceforther when we refer to 'saturation' we refer to this effect of saturating the density of states and not to a saturation of drift velocity. In the charge-carrier density saturation limit, the internal diffusion barrier height, $q\phi_{\mathrm{diff}}$, will be exactly equal to zero.

Assuming boundary conditions set through eq. 3 at the device edges, a constant charge-carrier density at the metal/semiconductor interfaces is achieved when the injection barriers and the effective density of states in the semiconductor (N_{C}) are specified,

$$n_{\text{interface}} = N_{\text{C}} \exp\left(-\frac{q\phi_{\text{inj}}}{k_{\text{B}}T}\right). \quad (6)$$

From this definition of the contacts the upper limit for the charge-carrier density at the boundaries will then be $n_{\text{interface}} = N_{\text{C}}$ given that the injection barriers are vanishing (and not negative).

The charge-carrier density inside the device, n, is given from the relative position of the semiconductor Fermi level, $E_{\text{F}}^{\text{s.c.}}$, and the conduction band edge, E_{C}, through,

$$n = N_{\text{C}} \exp\left(-\frac{E_{\text{C}} - E_{\text{F}}^{\text{s.c.}}}{k_{\text{B}}T}\right). \quad (7)$$

Neglecting injection barriers for the moment, when a large voltage is applied, and a large number of charge carriers are injected into the device from the electrodes ($E_{\text{C}} - E_{\text{F}}^{\text{s.c.}} \rightarrow 0$), the carrier density will tend towards uniformity across the entire thickness of the device ($n \rightarrow n_{\text{interface}} = N_{\text{C}}$). In this case, the semiconductor acts like a metal, the electric field inside the device is negligible, and the electric field across the semiconductor arise solely from the applied voltage, $F = V/L$, i.e., arising from the charge-carriers accumulated at the contacts. With the inclusion of injection barriers, the limit for saturation is given as $E_{\text{C}} - E_{\text{F}}^{\text{s.c.}} \rightarrow q\phi_{\text{inj}}$, and the saturation current density, in this high voltage limit, is given by[22][33][34],

$$J = q\mu_{\text{n}} N_{\text{C}} \frac{V}{L} \exp\left(-\frac{q\phi_{\text{inj}}}{k_{\text{B}}T}\right), \quad (8)$$

which is Ohm's law modified for injection limitation through eq. 6. Note that eq. 8 is only truly valid given that $q\phi_{\text{inj}} > 2k_{\text{B}}T$ (see fig. S1) and that velocity saturation can be ignored (which should be the case when $\phi_{\text{inj}} > 2k_{\text{B}}T$).

By comparing the three equations governing the low, intermediate and high voltage regimes, namely eq. 1, 2 and 8, it is obvious that several regimes can dominate the current density as a voltage is applied.

3.4. The Mark-Helfrich equation

One of the commonly used analytical equations which describes SCLC charge transport in a semiconductor with traps assumed in the form of localised charge carriers in exponential tails (fig. 2b),

$$h = n_{\text{t}} \exp\left(\frac{E}{E_{\text{ch}}}\right) \quad (9)$$

where n_{t} is the trap density per unit energy right below the band edge ($n_{\text{t}} = N_{\text{t}}/E_{\text{ch}}$ where N_{t} is the trap density), E_{ch} is the characteristic energy, and E is the energy measured from the transport level; is the Mark-Helfrich (MH) equation[7][9], which for an electron-only device is given by,

$$J = q^{1-l} \mu_{\text{n}} N_{\text{eff}} \left\{\frac{\varepsilon_{\text{r}}\varepsilon_0 l}{N_{\text{t}}(l+1)}\right\}^{l} \left\{\frac{2l+1}{l+1}\right\}^{l+1} \frac{V^{l+1}}{L^{2l+1}} \quad (10)$$

where q is the elementary charge, $l = E_{\text{ch}}/k_{\text{B}}T$, and N_{eff} is the effective density of states. Equation 10 correctly predicts that exponential tail states in the band gap give rise to a stronger power-law dependence of voltage on current than expected from the MG law in the intermediate voltage regime. However, it was recently shown that this equation is not accurate since it fails to account

for diffusion currents, which can make a significant contribution to the total current, especially when traps are present[12]. The Mark-Helfrich equation is however still a useful qualitative tool even though the equation is not quantitatively correct.

3.5. Slope analysis

It is common to plot SCLC current density-voltage profiles on a double logarithmic scale, since most information about the *J*-*V* curve is shown in this way. It is however convenient to monitor current regimes by considering the slope, m, of the current density-voltage curve on a log-log scale[33],

$$m = \frac{\mathrm{d}\log J}{\mathrm{d}\log V}. \qquad (11)$$

From this definition, the current density will depend on the power of the voltage through,

$$J \propto V^{m(V)}. \qquad (12)$$

The initial linear regime will then follow $m = 1$ (eq. 1), the MG law will have $m = 2$ (eq. 2), while the saturation current will again follow $m = 1$ (eq. 8). As will be shown in the results section, plotting *J*-*V* curves alongside *m*-*V* curves is a powerful tool when analysing SCLC.

3.6. Summary of the theory section

For the understanding of the results of this paper, the most important findings from the theory section are that even in the ideal, trap-free system, the current of a single-carrier device shows three regimes as a function of voltage. For low voltages, the *J*-*V* regime is linear due to moving electrode effect (eq. 1). For intermediate voltages, the MG law suggests that the current changes with V^2 (eq. 2). For high voltages, the charge density becomes spatially constant, and the current becomes Ohmic and depends on this spatially constant charge density given essentially by the density of states and the injection barrier heights (eq. 8). In the presence of traps, qualitatively the same effects happen but they are quantitatively affected by the charge carriers in the traps. The three regimes for different voltage ranges may be overlapping depending on thickness and injection barriers and therefore there may be situations where the intermediate regime needed for the application of the MG law partly disappears. The disappearance of the MG regime will be a central point for the results section of this paper, and is studied through the utilization of a drift-diffusion simulation solver.

4. Drift-diffusion simulations

The drift-diffusion simulations were performed using a commercially available device simulator called Advanced Semiconductor Analysis (*ASA*)[35]. *ASA* solves Poisson's equation numerically,

$$\nabla^2\varphi(x) = -\frac{\rho}{\varepsilon_0\varepsilon_\mathrm{r}}, \qquad (13)$$

along with the drift-diffusion equations for electrons and holes in one dimension,

$$-\frac{J_n(x)}{q} = -D_n\frac{dn(x)}{dx} - n(x)\mu_\mathrm{n}F(x), \qquad (14)$$

$$\frac{J_p(x)}{q} = -D_p\frac{dp(x)}{dx} + p(x)\mu_\mathrm{p}F(x). \qquad (15)$$

In the above three equations (eqs. 13, 14 and 15), φ is the electrical potential, ρ is the total charge density, J is the current density, D is the Einstein-Smoluchowski diffusion coefficient ($D = \mu k_B T/q$), n and p are the charge-carrier densities for either electrons or holes, and F is the electric field. Traps are modelled according to eq. 9, with the free and localised charge-carrier populations governed by Shockley-Read-Hall statistics[8][31][36]. The boundary conditions are set by the injection barrier heights through eq. 6. Electron-only devices with Ohmic contacts ($q\phi_{\mathrm{inj}} = 0$ eV) and non-Ohmic contacts ($q\phi_{\mathrm{inj}} > 0$ eV) for both injection and extraction (simultaneously) are considered. It should here be noted that some error is introduced when using Boltzmann statistics, rather than Fermi-Dirac statistics, close to degeneracy. However, since for most realistic cases $q\phi_{\mathrm{inj}} > 2k_{\mathrm{B}}T$ eV anyway, we will use Boltzmann statistics for the numerical analysis (see fig. S1). Furthermore, it is not possible to evaluate the integrals for the analytical derivations when using Fermi-Dirac statistics (eq. S15). The relative permittivity, ε_{r}, for conjugated organic materials is often cited to be around 3[31][37][38], which is much less than for many frequently used inorganic semiconductors (> 10)[39] or lead halide perovskite materials (~ 30)[40]. We will later show how the choice of dielectric constant value affects the results. Charge carrier mobilities differ strongly with the choice of material, however, when a sole charge-carrier type is present, recombination can be neglected, and for that reason the charge mobility only affects the magnitude of the current and not the regime transitions (see fig. S2). Since typical values in organic materials used for organic photovoltaics are around $\mu_{\mathrm{e}} = 10^{-4}$ cm^2/Vs, we will rather arbitrarily use this as a value. The effective density of states for organic materials is not well defined, but values are typically cited to be around $N_{\mathrm{C}} = N_{\mathrm{V}} = 10^{19}$ cm^{-3}[8][31][41], which is not too different from the values cited for inorganic materials. The band-gap of semiconductors used for solar cells range between 1.1 eV and 2.1 eV, so the simulations will arbitrarily be conducted on a representative 2 eV band-gap material. The value of the band gap only affects the magnitude of the intrinsic charge-carrier density, which will still be much less than the magnitude of the equilibrium charge-carrier density[27]. The series resistance potentially arising from the contacts, and the shunt resistance which is important in the case where a large number of pinholes are present, are neglected in this discussion. Neglecting the shunt resistance is a fair assumption since shunt currents mostly manifest themselves at low voltages when a large built-in voltage is present in the device. The series resistance can be neglected when the product of the equilibrium charge-carrier density and mobility of the semiconductor is low relative to the conductivity of the contact electrodes, which is usually the case for low mobility semiconductors. Bipolar transport is not considered (bipolar devices represent a separate case with its own pitfalls and we do not address these in this paper). For all simulations the temperature, T, is assumed to be $T = 300$ K.

5. Simulation results

The analytical equations governing the low, intermediate and high voltage regimes (eqs. 1, 2 and 8, respectively) are compared to numerical drift-diffusion simulations of intrinsic semiconductors in either ideal (Ohmic) or non-ideal (non-Ohmic) single-carrier devices. Because the results will depend strongly on the thickness of the device, we will present most data for 50, 100 and 500 nm devices.

5.1. Ohmic contacts

Figure 3a shows *J*-*V* profiles of trap free 50, 100 and 500 nm electron-only devices with Ohmic contacts ($q\phi = 0.0$ eV). Fits with the ME equation (eq. 1) and the MG law (eq. 2) to the 500 nm device is shown as solid lines. Figure 3b shows *J*-*V* profiles of electron-only devices with Ohmic contacts and traps in the form of exponential tails states extending from the transport levels, i.e., from the conduction and valence band edges ($E_{\mathrm{ch}} = 0.05$ eV and $n_{\mathrm{t}} = 10^{20}$ cm^{-3}eV^{-1}). Figure 3c

shows the slopes (eq. 11) of the J-V curves in figs. 3a and b as a function of voltage. For the trap free single-carrier devices, the onset for the increase in the slope away from a linear dependence ($m = 1$) at low voltages occur at the same voltage, V_X, for all three thicknesses. It is also seen, that for a 50 nm device, the slope does not reach, and retain, a value of $m = 2$ but rather $m = 1.9$, which decreases towards unity. As the thickness of the semiconductor is increased to 100 nm, the maximum slope increases ($m = 1.95$), but also tends back towards unity at high voltages. For the devices containing traps, the slope is seen increase to above $m = 2$ for all three thicknesses, but does not reach the same value for the maximum slope value. The MH equation (eq. 10) predicts that $m = 1 + E_{ch}/k_B T$, which would reach a value of $m = 2.92$ for all three thicknesses. However, the values for the slope maxima are $m = 2.56$ and $m = 2.70$ for the 50 and 100 nm device respectively and is approaching what is expected from the Mark-Helfrich equation for the 500 nm device ($m = 2.86$). Figure 3d shows the maximum slope values for a series of single-carrier devices as a function of increased thicknesses and dielectric constants. The deviation of the slope maximum from $m = 2$ is seen to be more profound as the dielectric constant is increased towards values typical for inorganic and hybrid semiconductors.

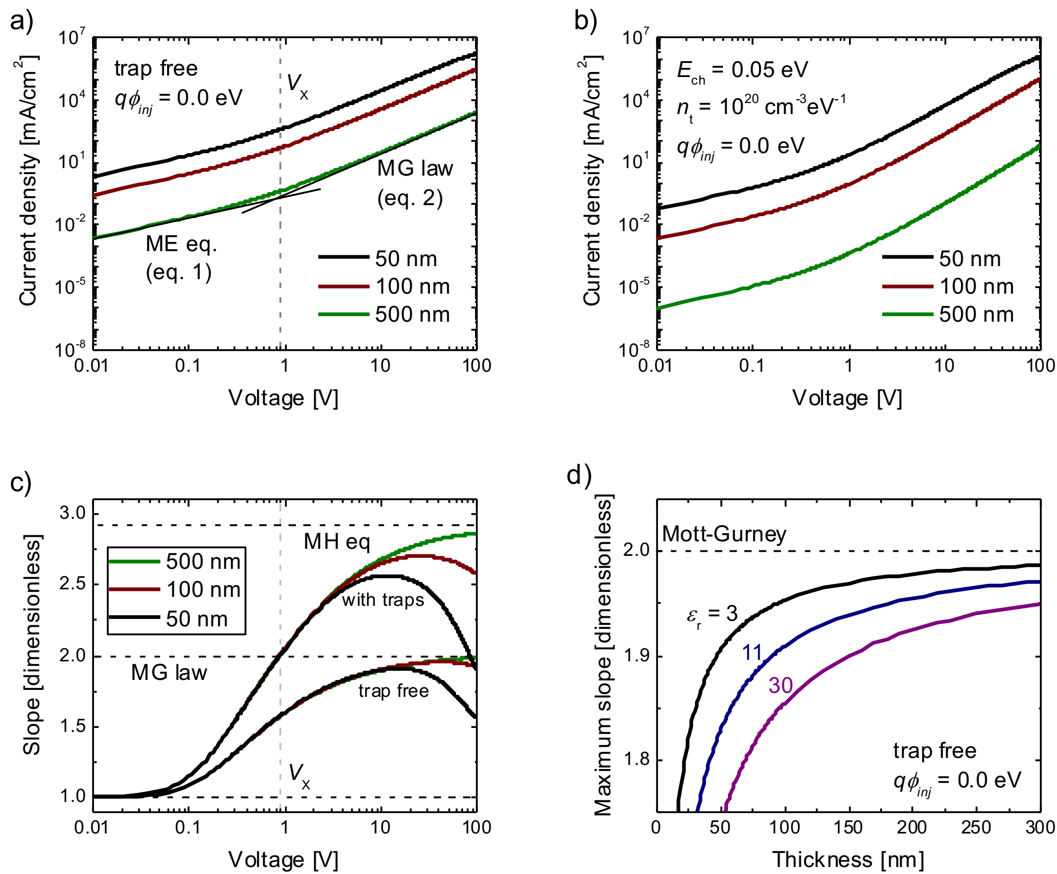

Figure 3 – a) Numerically calculated current density-voltage profiles for trap free 50, 100 and 500 nm electron-only devices with Ohmic injection. Fits with the ME equation (eq. 1) and the MG law (eq. 2) are shown as solid lines. b) Current density-voltage profiles for 50, 100 and 500 nm electron-only devices with Ohmic injection and traps (E_{ch} = 0.05 eV, $n_t = 10^{20}$ cm^{-3}eV^{-1}). c) Slope-voltage profiles showing the voltage of the onset to drift dominated currents, V_X (the expected slopes for the MG law and the MH eq. are shown as dashed lines). d) Maximum slope for devices with increasing thickness showing the deviation of the slope from the value of 2 (dashed line) for the cases of a dielectric constant similar to organic (ε_r = 3, solid line), inorganic (ε_r = 11, dot-dashed line) and lead-halide perovskites (ε_r = 30, dotted line).

5.2. Non-Ohmic contacts

The numerical results shown in fig. 3 are for the cases of ideal devices, where perfect injection is achieved through Ohmic contacts. However, a more realistic case will be when the injection contacts are non-Ohmic, i.e., the injection barriers at the device boundaries are finite, $q\phi_{\mathrm{inj}} > 0$ eV.

It has previously been reported that devices with 0.2 eV barrier heights still show nearly Ohmic carrier injection[42]. The effect of injection barriers heights is however highly dependent on the thickness of the probed semiconductor, and a thin device (50 nm) will be influenced to a higher degree than a thick device (500 nm) as seen in fig. S3. Figure 4a shows the slope of a 100 nm device as the injection and extraction barriers are simultaneously increased (0, 0.026, 0.052, 0.1 and 0.2 eV). The maximum slope value decreases with increasing injection barrier height while the slope maximum position shifts to lower voltages. A transition to a linear regime at high voltages is observed. Figure 4b shows that the voltage of the transition to the linear regime scales with L^{-2}, and fig. 4c shows that the transition scales with an exponential term containing the injection barrier height.

Figure 3c shows that the maximum slope increases beyond $m = 2$ when a significant density of traps is present. However, fig. 4d shows that with a combination of traps and injection limitation a slope maximum with $m < 2$ can be achieved. From this it is clear that with a certain combination of traps and injection limitation $m = 2$ could be achieved leading to a wrongful analysis with the MG law.

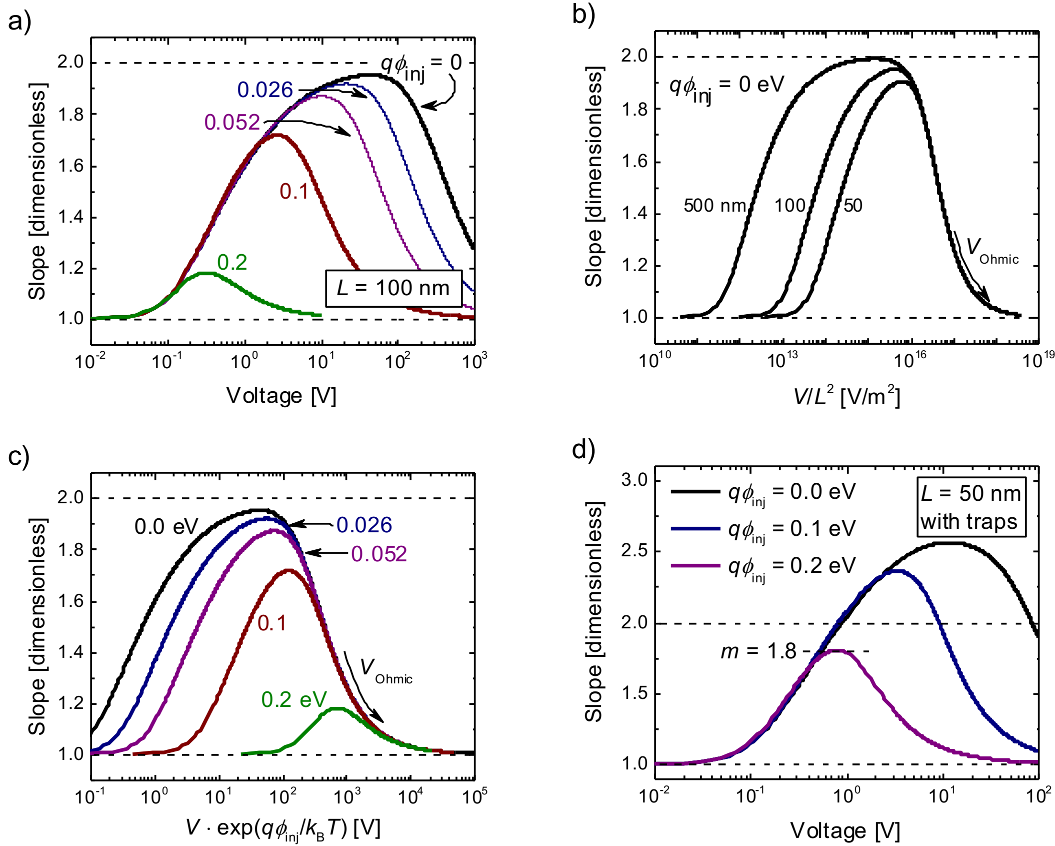

Figure 4 – a) Slope-voltage curves of a 100 nm device with increasing injection barriers. b) Slope as a function of $\boldsymbol{V/L^2}$ for thicknesses of 50, 100 and 500 nm electron only devices. The voltage axis was corrected in order to show $\boldsymbol{L^2}$ scaling for the transition to Ohmic saturation currents (eq. 17). c) Slopes of a 100 nm device with increasing injection barriers when the voltage axis is corrected for by the exponential term governing injection limitation (eq. 6). The voltage onset

for Ohmic currents is seen to scale accordingly, further validating eq. 17. d) Slope-voltage curves of a 50 nm device with injection limitation and exponential band tails (E_{ch} = 0.05 eV, n_t = 10^{20} cm^{-3}eV^{-1}).

5.3. *Fitting with the Mott-Gurney law and the moving electrode equation*

The MG law can only be fitted to *J*-*V* curves where a slope of 2 is observed. In figs. 3b and c, and in fig. 4a it is seen that in the case of a device with a realistic thickness and injection barriers, a slope of 2 is never observed. Despite it being impossible to fit the MG law even in the ideal case, and even less so for devices with realistic contacts, the MG law might still yield reasonable results if the mobility is calculated using values for the voltage and current density around the region of maximum slope. This means, that eq. 2 is evaluated at $V = V(m_{\text{max}})$. This will, of course, cause this "fit" with the MG law to intersect the *J*-*V* curve (since the MG has m = 2 and m_{max} < 2 even for the thin ideal devices).

In order to assess the error introduced when using eq. 1 or eq. 2 to obtain the charge carrier mobility, the equations were "fitted" to numerically calculated *J*-*V* curves in the case of Ohmic and non-Ohmic contacts as a function of the active layer thickness.

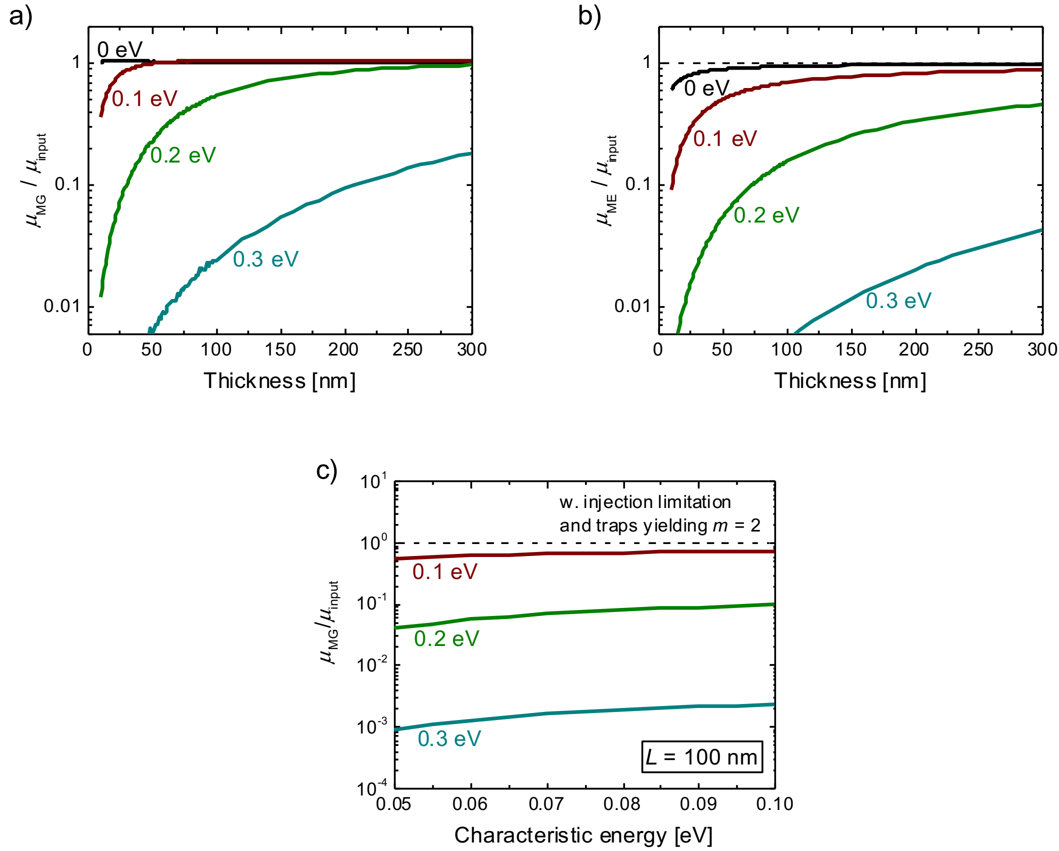

Figure 5 – Extracted mobility using analytical equations when the injection barriers are increased (0.1, 0.2 & 0.3 eV); a) extraction of mobility when fitting with the MG law at the slope maximum, and b) extraction of the mobility when fitting with the moving-electrode equation (eq. 5). The values are normalized with respect to the input value for the mobility. c) Fitting results with the MG law when $\boldsymbol{m} = \mathbf{2}$ due to a combination of tail states and injection barriers (as shown in fig. S4).

Figure 5a shows the obtained charge-carrier mobility when fitting with the MG law (eq. 2) relative to the electron mobility used as an input (μ_{input} = 10^{-4} cm^2/Vs). Figure 5b is the equivalent graph

for fitting with the ME equation (eq. 1). The ME equation was fitted between 0 and 0.1 V, as this range is seen to be linear for both cases (see figs. 3b & 4a). However, this fit is not always physically correct, as non-Ohmic contacts reduce the overall current and the ME equation cannot account for this. For Ohmic contacts it is seen that both eqs. 1 and 2 yield good results even at very small thicknesses (~ 10 nm). That the MG law yields good results is rather surprising since the slope maximum in this case is 1.6, i.e., substantially less than $m = 2$. The predicted mobility when using eq. 1 is, surprisingly, less correct as compared to using eq. 2. It is seen that when small injection barriers are added ($\phi_{\text{inj}} = 0.1$ eV), even though the slope maximum will not reach $m = 2$, the mobility can still be estimated within a reasonable accuracy using the MG law, provided that the device is not too thin (> 50 nm). When the injection barriers are increased to 0.2 eV, the MG law significantly deviates for small thicknesses, whereas the ME equation deviates at all thicknesses investigated here. With 0.3 eV barrier heights, both equations deviate dramatically for the calculated thicknesses. Figure 5c shows the ratio of the obtained mobility using the MG law to the input mobility when traps and injection limitation were included in a 100 nm device in order to force $m = 2$ (the trap characteristics that were needed for the resulting J-V curve to have m = 2 were different in each case and are shown in fig S4). It is quite apparent that the mobility can be greatly underestimated even though the equation was fitted to a J-V curve that appeared to be obtained from an ideal device.

6. Analytical results

In order to give an analytical explanation to the drop in the maximum slope from $m = 2$ to much lower values at intermediate voltages, the cross-over voltages, denoting the transition between transport regimes, are discussed.

6.1. Transition from low voltage to the Mott-Gurney regime

The temperature dependent cross-over voltage between the low voltage regime and the MG regime, observed in figs. 3a and c, has previously been derived, by equating the ME equation (eq. 1) with the MG law (eq. 2), to be[30],

$$V_{\text{X}} = \frac{32\pi^2}{9}\frac{k_{\text{B}}T}{q}. \quad (16)$$

This equation replaced the onset equation, $V_{\text{X}} = (8/9)\{(nqL^2)/(\varepsilon_0\varepsilon_{\text{r}})\}$, derived by Mark & Lampert (which stated that the onset was thickness dependent) when dealing with symmetric single-carrier devices of intrinsic semiconductors with Ohmic contacts[13]. At room temperature, the onset voltage, eq. 16, approximately gives 0.9 V, and is not affected by the magnitude of injection barriers (see fig. 4a).

6.2. Transition from the Mott-Gurney regime to saturation

The cross-over voltage from the MG regime to the saturation regime can be derived by equating the MG law (eq. 2), with the saturation current equation (eq. 8), which includes a term accounting for the reduction of the charge-carrier density at the boundaries due to poor injection,

$$V_{\text{sat}} = \frac{8}{9}\frac{qL^2}{\varepsilon_0\varepsilon_{\text{r}}}N_{\text{C}}\exp\left(-\frac{q\phi_{\text{inj}}}{k_{\text{B}}T}\right). \quad (17)$$

From eq. 17 is seen that the onset to the Ohmic saturation current follows an L^2 thickness scaling, which is also seen from the numerical calculations in fig. 4b. Contrary to the onset from the low voltage regime to the MG regime, eq. 16, the effect of the injection barriers is to shift the cross-over voltage by the exponential term. This effect is seen from the numerical calculation in fig. 4c.

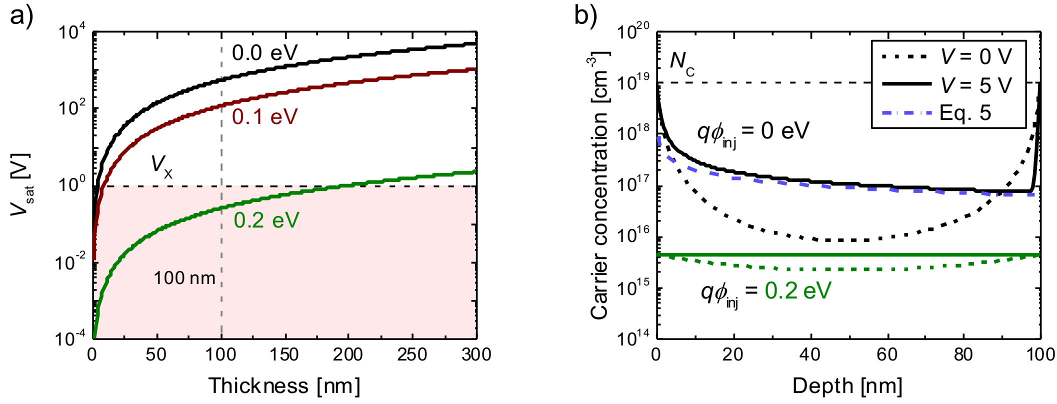

Figure 6 - a) V_{sat} as a function of device thickness with varying injection barrier heights (0, 0.1 and 0.2 eV). The onset to the MG regime, V_X, is shown as a black dashed line. V_{sat}(0.0 eV, 100 nm) = 53.6 V, whereas V_{sat}(0.2 eV, 100 nm) = 0.2446 V, i.e., much lower than V_X = 0.9 V. The pink region shows the situation where the two linear regimes overlap and the MG law cannot express the intermediate voltage regime. b) Electron concentration at 0 V (dashed lines) and 5 V (solid lines) in a 100 nm device with and without injection barriers, as shown by black colours and green colours (the value for the effective density of states is shown for reference). The carrier density as calculated from eq. 5 is shown as a dot-dashed blue line.

Figure 6a shows calculations of eq. 17 as a function of device thickness with either perfect injection through Ohmic contacts, $q\phi_{\text{inj}} = 0.0$ eV, or with non-Ohmic contacts with a small injection barrier, $q\phi_{\text{inj}} = 0.1$ eV or 0.2 eV. The thickness independent cross-over voltage to the MG regime, V_X, is shown by the black dashed line. It is seen that, under certain conditions, the onset to the saturation current is occurring before the current has transitioned into the MG regime. To supplement this, fig. 6b shows that when 5 V is applied across a 100 nm device with Ohmic contacts, the electron density in the device approximately follows the electron density derived from assuming drift-only transport (eq. 5), i.e., the current approximately follows the MG law. On the contrary, when 5 V is applied to an injection limited device (0.2 injection barriers), the electron density is completely uniform across the depth of the device, i.e., the current regime has transitioned into saturation without transitioning through the MG regime.

6.3. *Maximum slope*

The average value of the MG charge-carrier concentration (eq. 5) is given by,

$$\langle n \rangle_{\text{MG}} = \frac{1}{L}\int_0^L \frac{1}{q}\sqrt{\frac{J\varepsilon_0\varepsilon_{\text{r}}}{2\mu_n x}}\,\mathrm{d}x, \qquad (18)$$

which yields an equation for the voltage at the slope maximum, V_{Max},

$$V_{\text{Max}} = \frac{4}{6}\frac{qL^2\langle n \rangle_{\text{MG}}}{\varepsilon_0\varepsilon_{\text{r}}}. \qquad (19)$$

The voltage values predicted from eq. 19 coincide with the maximum slopes from the numerical calculations in fig. 3c. The previous SCLC onset by Mark & Lampert predicted that the onset from the low voltage regime to the MG regime follows a L^2 scaling. However, we can see from eqs. 17 and 19, that it is the maximum value for the slope and the transition to the Ohmic saturation regime that follows the L^2 scaling rather than the onset to the MG regime. Moreover, eq. 19 predicts that the maximum slope shifts to lower voltages when the carrier density decreases (with a fixed thickness), which is what is observed in fig. 4a.

7. Discussion

We observe that for practically relevant thicknesses (100 nm) there is a slight deviation from the behaviour predicted by the MG law when no injection barriers are present (see figs. 3c and d). This deviation is sensitive to thickness as shown by the calculated behaviour of a 50 nm thick film which shows a larger deviation from the MG law than either a 100 or a 500 nm film (figs. 3c and d). However, the deviation from the MG law becomes strikingly relevant as soon as one considers practically relevant injection barriers (see figs. 4a and 5a) even for a 100 nm device.

When a large voltage is applied across a thin device (50 nm) with Ohmic contacts, it is seen that the current is dominated by saturation of the charge-carrier density (see fig. 3b). Even though the transition to complete saturation happens at a very high voltage, the maximum value of the slope is reduced to around $m = 1.9$. The reduction in the slope value makes a fit with the MG law impossible. Even though the reduction in the slope maximum away from $m = 2$ for a 50 nm device with Ohmic contacts is more apparent than for a 100 nm, some deviation is still seen for the 100 nm device (see fig. 3c).

With injection barriers introduced at the interfaces, a dramatic reduction of the maximum slope values is observed (see fig. 4a). Interestingly, the cross-over voltage from the linear regime at low voltage is seen to be neither affected by the thickness of the device nor the injection barrier heights (see figs. 3c and 4a). This observation from the numerical calculations agrees with eq. 16. Furthermore, the position of the maximum slope value shifts to lower values for the voltage both when the thickness is reduced and when injection barriers are increased. This is explained from a reduction in the charge-carrier density and agrees with eq. 19.

From figs. 4b and c it is seen that the onset to the saturation regime, V_{sat}, changes both with thickness and injection barrier heights. This agrees with eq. 17. Figure 6a shows comparisons of calculations of V_{sat} with varying injection barrier heights to V_{X}. When V_{sat} is roughly equal to or lower than the voltage onset to V_{X}, a lowering of the slope away from $m = 2$ at all voltages is observed. This is because the current has transitioned into the saturation regime before becoming a space-charge-limited drift current, i.e., the two linear regimes overlap and the MG regime has disappeared (see fig. 6b). In fig. 6a it is also seen that the value for V_{sat} is close to V_{X} for the 10 nm device with Ohmic contacts, whereas the 100 nm device has a much higher onset voltage to saturation currents. This explains why the slope of a thin device has a low maximum value around, where a thicker device has a maximum value approaching $m = 2$.

The effect of the slope maximum lowering was seen to be even more profound when realistic (non-Ohmic) contacts are used (see fig. 4a). The lowering of the slope is assigned to the carrier concentration being almost uniform even before a voltage is applied (see fig. 6b). When electrons are injected into the almost saturated device, the charge carrier density will then quickly tend towards uniformity, and the current will follow eq. 8 at a much lower voltage ($V_{\mathrm{Ohmic}} < 1$ V for a 100 nm device when $q\phi_{\mathrm{inj}} = 0.2$ eV). So even for ideal semiconductors, this transition to saturation currents, which happens at very low voltages for devices with a realistic semiconductor thickness and realistic injection barriers, makes fitting with the MG law meaningless since the current density is never proportional to V^2. This also means that if $m \geq 2$ is observed for thin devices, then an extrinsic mechanism such as traps or energetic disorder must be present, and in such cases the MG law is again not applicable since this model was developed for intrinsic semiconductors (see fig. 4d). Furthermore, if $m = 2$ is in fact observed for reasonably thin devices, a combination of traps and injection limitation could be present in the device, rendering analysis with the MG law meaningless regardless (see fig. 5c).

If the MG law is used to fit to SCLC J-V curves when small injection barriers (0.1 eV) are present, the obtained mobility will not deviate dramatically given that the thickness of the probed semiconductor is larger than 50 nm (see fig. 5a). For slightly larger injection barriers (0.2 eV) an underestimation of the mobility of almost an order of magnitude can be expected for a 50 nm

device. Measuring a thicker device (100 nm) will yield a more accurate value for the mobility, but will still be underestimated.

In practice, SCLC active layer thicknesses are usually of order of 50 nm or above, but they may suffer injection barriers of several tenths of an eV due to limited range of available contacts[38]. Moreover, practical devices usually contain some density of traps[17]. Therefore the risks that we highlight here in the interpretation of SCLC data using the MG law are relevant for common practice in mobility estimation, especially with organic semiconductors. Figures 5 and 6 in combination can be used as a helpful tool to predict when, and by how much, the charge-carrier mobility will be wrongly estimated when either using the MG law or the ME equation when using devices without Ohmic contacts to measure semiconductors with or without some degree of trapping.

8. Conclusions

By comparing the results from the analytical equations with numerical calculations it is shown that a strong deviation from the Mott-Gurney law towards an Ohmic saturation current is seen when simulating single-carrier devices of intrinsic semiconductors with realistic (non-Ohmic) injection contacts. This is shown to be due to an increased accumulation and eventual saturation of charge carriers inside the device when a voltage is applied. The onset for these Ohmic currents is shown to follow a square scaling law with thickness and an exponential scaling law with injection barrier heights, meaning that this phenomenon is even more profound, and occurring at even lower voltages, when the device thickness of the material is decreased and/or when the injection barrier heights are increased towards realistic values. The thinner the device and larger the injection barriers, the more difficult it becomes to fit the Mott-Gurney law to the current density-voltage curves, and the larger the deviation of the obtained mobility values compared to the real mobility values becomes. The deviation of the charge carrier mobility when determined using the Mott-Gurney law, or the Moving Electrode equation, is quantified, and it is shown that the mobility can be underestimated by several orders of magnitude compared to when obtained using numerical fitting. In order to use the discussed analytical expressions for analysis of SCLC data from intrinsic single-carrier devices, it is important to minimize injection barriers and to measure devices with thicknesses larger than 50 nm. This analysis can be used to help design the correct device architecture for charge-carrier mobility measurements while help to estimate the error involved in the extracted values when measuring intrinsic semiconductors.

9. Acknowledgements

JAR, SAH, DM and JN would like to thank the Engineering and Physical Sciences Research Council (EPSRC grant nos. EP/K030671/1 and EP/K010298/1) and the Centre of Doctoral Training on Plastic Electronics (EP/G037515) for funding. JAR would like to thank Dr. Piers Barnes, Dr. Alasdair Campbell, Dr. Xingyuan Shi and Ms. Suki Wong for fruitful discussions.

10. References

[1] R. W. Smith and A. Rose, "Space-Charge-Limited Currents in Single Crystals of Cadmium Sulfide," *Phys. Rev.*, vol. 97, no. 6, pp. 1531–1537, 1955.

[2] M.-H. Chen *et al.*, "Efficient Polymer Solar Cells with Thin Active Layers Based on Alternating Polyfluorene Copolymer/Fullerene Bulk Heterojunctions," *Adv. Mater.*, vol. 21, no. 42, pp. 4238–4242, Nov. 2009.

[3] R. Steyrleuthner *et al.*, "Bulk Electron Transport and Charge Injection in a High Mobility n-Type Semiconducting Polymer," *Adv. Mater.*, vol. 22, no. 25, pp. 2799–2803, Jul. 2010.

[4] Z. He *et al.*, "Simultaneous Enhancement of Open-Circuit Voltage, Short-Circuit Current Density, and Fill Factor in Polymer Solar Cells.," *Adv. Mater.*, vol. 23, no. 40, pp. 4636–43, Oct. 2011.

[5] J. C. Blakesley *et al.*, "Towards Reliable Charge-Mobility Benchmark Measurements for Organic Semiconductors," *Org. Electron.*, vol. 15, no. 6, pp. 1263–1272, 2014.

[6] N. F. Mott and R. W. Gurney, *Electronic Processes in Ionic Crystals*. Oxford University Press, 1940.

[7] P. Mark and W. Helfrich, "Space-Charge-Limited Currents in Organic Crystals," *J. Appl. Phys.*, vol. 33, no. 1, pp. 205–215, 1962.

[8] T. Kirchartz, "Influence of Diffusion on Space-Charge-Limited Current Measurements in Organic Semiconductors.," *Beilstein J. Nanotechnol.*, vol. 4, pp. 180–188, Jan. 2013.

[9] A. Rose, "Space-Charge-Limited Currents in Solids," *Phys. Rev.*, vol. 97, no. 6, pp. 1538–1544, Mar. 1955.

[10] M. A. Lampert, "Simplified Theory of Space-Charge-Limited Currents in an Insulator with Traps," *Phys. Rev.*, vol. 103, no. 6, pp. 1648–1656, 1956.

[11] P. N. Murgatroyd, "Theory of Space-Charge-Limited Current Enhanced by Frenkel Effect," *J. Phys. D Appl. Phys.*, vol. 3, pp. 151–156, 1970.

[12] J. Fischer, W. Tress, H. Kleemann, J. Widmer, K. Leo, and M. Riede, "Exploiting Diffusion Currents at Ohmic Contacts for Trap Characterization in Organic Semiconductors," *Org. Electron.*, vol. 15, no. 10, pp. 2428–2432, Oct. 2014.

[13] M. Lampert and P. Mark, *Current Injections in Solids*. Academic Press, 1970.

[14] N. I. Craciun, J. J. Brondijk, and P. W. M. Blom, "Diffusion-Enhanced Hole Transport in Thin Polymer Light-Emitting Diodes," *Phys. Rev. B*, vol. 77, p. 035206(1-5), 2008.

[15] H. T. Nicolai, M. M. Mandoc, and P. W. M. Blom, "Electron Traps in Semiconducting Polymers: Exponential versus Gaussian Trap Distribution," *Phys. Rev. B*, vol. 83, no. 19, p. 195204, May 2011.

[16] J. Dacuña and A. Salleo, "Modeling space-charge-limited currents in organic semiconductors: Extracting trap density and mobility," *Phys. Rev. B*, vol. 84, no. 19, p. 195209, Nov. 2011.

[17] H. T. Nicolai *et al.*, "Unification of trap-limited electron transport in semiconducting polymers.," *Nat. Mater.*, vol. 11, no. 10, pp. 882–7, Oct. 2012.

[18] J. Dacuña, W. Xie, and A. Salleo, "Estimation of the Spatial Distribution of Traps using Space-Charge-Limited Current Measurements in an Organic Single Crystal," *Phys. Rev. B*, vol. 86, no. 11, p. 115202, Sep. 2012.

[19] S. Holliday *et al.*, "A Rhodanine Flanked Nonfullerene Acceptor for Solution-Processed Organic Photovoltaics," *J. Am. Chem. Soc.*, vol. 137, no. 2, pp. 898–904, Jan. 2015.

[20] R. de Levie, N. G. Seidah, and H. Moreia, "Transport of Ions of One Kind through Thin Membranes," *J. Membr. Biol.*, vol. 10, pp. 171–192, 1972.

[21] A. A. Grinberg and S. Luryi, "Space-Charge-Limited Current and Capacitance in Double-Junction Diodes," *J. Appl. Phys.*, vol. 61, no. 3, pp. 1181–1189, 1987.

[22] J. G. Simmons, "Richardson-Schottky Effect in Solids," *Phys. Rev. Lett.*, vol. 15, no. 25, pp. 967–968, 1965.

[23] D. Baran *et al.*, "Reducing the efficiency-stability-cost gap of organic photovoltaics with highly efficient and stable small molecule acceptor ternary solar cells," *Nat. Mater.*, vol. 16, no. 3, pp. 363–369, 2017.

[24] H. K. H. Lee *et al.*, "The Role of Fullerenes in Environmental Stability of Polymer:Fullerene Solar Cells," *Energy Environ. Sci.*, 2017.

[25] J. G. Simmons, "Theory of Metallic Contacts on High Resistivity Solids - I. Shallow Traps," *J. Phys. Chem. Solids*, vol. 32, pp. 1987–1999, 1971.

[26] H. K. Henisch, *Semiconductor Contacts: An Approach to Ideas and Models*, 1st ed. Oxford Science Publications, 1984.

[27] J. A. Röhr, T. Kirchartz, and J. Nelson, "On the Correct Interpretation of the Low Voltage Regime in Intrinsic Single-Carrier Devices," *J. Phys. Condens. Matter*, vol. 29, no. 20, p. 205901(9), 2017.

[28] J. C. Scott and G. G. Malliaras, "Charge Injection and Recombination at the Metal – Organic Interface," *Chem. Phys. Lett.*, vol. 299, no. January, pp. 115–119, 1999.

[29] G. a. H. Wetzelaer and P. W. M. Blom, "Ohmic Current in Organic Metal-Insulator-Metal Diodes Revisited," *Phys. Rev. B*, vol. 89, no. 24, p. 241201, Jun. 2014.

[30] S. L. M. van Mensfoort and R. Coehoorn, "Effect of Gaussian Disorder on the Voltage Dependence of the Current Density in Sandwich-Type Devices based on Organic Semiconductors," *Phys. Rev. B*, vol. 78, p. 085207(16), 2008.

[31] T. Kirchartz, B. E. Pieters, J. Kirkpatrick, U. Rau, and J. Nelson, "Recombination Via Tail States in Polythiophene:Fullerene Solar Cells," *Phys. Rev. B*, vol. 83, no. 11, p. 115209, Mar. 2011.

[32] F. Deledalle *et al.*, "Understanding the Effect of Unintentional Doping on Transport Optimization and Analysis

in Efficient Organic Bulk-Heterojunction Solar Cells," *Phys. Rev. X*, vol. 5, no. 1, p. 11032, Mar. 2015.

[33] M. Kryszewski and A. Szymański, "Space Charge Limited Currents in Polymers," *J. Polym. Sci. Macromol. Rev.*, vol. 4, no. 1, pp. 245–320, 1970.

[34] H. Scher, D. Pai, and J. Mort, "Criterion for determining the origin of Ohmic currents in insulators," *J. Appl. Phys.*, vol. 44, no. 6, pp. 2908–2909, 1973.

[35] M. Zeman and J. Krc, "Optical and Electrical Modeling of Thin-Film Silicon Solar Cells," *J. Mater. Res.*, vol. 23, no. 4, pp. 889–898, Jan. 2011.

[36] W. Shockley and W. T. Read, "Statistics of the Recombinations of Holes and Electrons," *Phys. Rev.*, vol. 87, no. 5, pp. 835–842, 1952.

[37] K. K. H. Chan, S. W. Tsang, H. K. H. Lee, F. So, and S. K. So, "Charge Injection and Transport Studies of Poly(2,7-carbazole) Copolymer PCDTBT and Their Relationship to Solar Cell Performance," *Org. Electron.*, vol. 13, no. 5, pp. 850–855, May 2012.

[38] D. Poplavskyy and J. Nelson, "Nondispersive Hole Transport in Amorphous Films of Methoxy-Spirofluorene-Arylamine Organic Compound," *J. Appl. Phys.*, vol. 93, no. 1, p. 341, 2003.

[39] I. Strzalkowski, S. Joshi, and C. R. Crowell, "Dielectric Constant and its Temperature Dependence for GaAs, CdTe, and ZnSe," *Appl. Phys. Lett.*, vol. 28, no. 6, p. 350, 1976.

[40] F. Brivio, A. B. Walker, and A. Walsh, "Structural and Electronic Properties of Hybrid Perovskites for High-Efficiency Thin-Film Photovoltaics from First-Principles," *APL Mater.*, vol. 1, no. 4, p. 42111, 2013.

[41] G. R. Hutchison, Y. Zhao, B. Delley, A. J. Freeman, M. A. Ratner, and T. J. Marks, "Electronic Structure of Conducting Polymers : Limitations of Oligomer Extrapolation Approximations and Effects of Heteroatoms," *Phys. Rev. B*, vol. 68, p. 035204(13), 2003.

[42] A. K. Mahapatro and S. Ghosh, "Schottky Energy Barrier and Charge Injection in Metal/Copper–Phthalocyanine/Metal Structures," *Appl. Phys. Lett.*, vol. 80, no. 25, p. 4840, 2002.